

Dimension reduction with mode transformations: Simulating two-dimensional fermionic condensed matter systems with matrix-product states

C. Krumnow,¹ L. Veis,² J. Eisert,^{1,3} and Ö. Legeza⁴

¹*Dahlem Center for Complex Quantum Systems, Freie Universität Berlin, 14195 Berlin, Germany*

²*J. Heyrovský Institute of Physical Chemistry, Academy of Sciences of the Czech Republic, Dolejškova 3, 18223 Prague 8, Czech Republic*

³*Department of Mathematics and Computer Science, Freie Universität Berlin, Germany*

⁴*Wigner Research Centre for Physics, Hungarian Academy of Sciences, Budapest, Hungary*

(Dated: December 15, 2024)

Tensor network methods have progressed from variational techniques based on matrix-product states able to compute properties of one-dimensional condensed-matter lattice models into methods rooted in more elaborate states such as projected entangled pair states aimed at simulating the physics of two-dimensional models. In this work, we advocate the paradigm that for two-dimensional fermionic models, matrix-product states are still applicable to significantly higher accuracy levels than direct embeddings into one-dimensional systems allow for. To do so, we exploit schemes of fermionic mode transformations and overcome the prejudice that one-dimensional embeddings need to be local. This approach takes the insight seriously that the suitable exploitation of both the manifold of matrix-product states and the unitary manifold of mode transformations can more accurately capture the natural correlation structure. By demonstrating the residual low levels of entanglement in emerging modes, we show that matrix-product states can describe ground states strikingly well. The power of the approach is exemplified by investigating a phase transition of spin-less fermions for lattice sizes up to 10×10 .

Recent years have enjoyed a flourishing development of tensor network methods, entanglement-based methods that allow to describe strongly correlated quantum many-body systems [1–5]. They originate from the powerful density-matrix renormalization group (DMRG) [6–8], a variational method building on matrix-product states (MPS) [9–11] that captures the physics of one-dimensional local Hamiltonian systems provably well [2, 12–14]. It has been applied to countless physical systems (see the reviews [8, 15] and the comprehensive web page [16]) and extended to time-evolving systems [17–19], open systems [20, 21], and the study of excited states [22]. Generalizing the variational set of matrix-product states to projected entangled pair states in two spatial dimensions, new avenues for the study of strongly correlated systems with tensor networks followed [1, 2, 23], including studies of fermionic models [24–27].

And yet, even if the DMRG approach has originally been devised to capture one-dimensional systems only: There are regimes in which it interestingly still performs competitively well [28, 29] even in situations that at first seem alien to that type of approach and in which area laws for entanglement entropies are violated [5]. Two-dimensional strongly correlated systems can be naturally embedded in highly non-local Hamiltonian models on a line. The high degree of entanglement that renders a variational approach based on matrix-product states challenging are partially compensated by the facts that contraction is efficient, and that very large bond dimensions are accessible. DMRG produces relevant data for strongly correlated matter even in two spatial dimensions, and for systems with fermionic degrees of freedom [30]. The significance of this insight is even strengthened by the fact that DMRG is strictly variational, so that all ground state energies generated are upper bounds. And yet, given that the entanglement structure is not fully captured by matrix-product states, there are strong limitations of direct DMRG approaches.

In this work, we bring the idea of tackling two-dimensional strongly correlated matter with effectively one-dimensional matrix-product states to a new level. We show that the potential of an effective dimensional reduction is significantly more powerful than anticipated. We do so by systematically exploiting a degree of freedom that has not sufficiently been appreciated in the study of strongly correlated condensed-matter systems: This is the degree of freedom to adaptively define suitable modes in a strongly correlated fermionic system. Its significance is already manifest when solving problems in either real or in momentum space [31–38]. For n fermionic modes, however, there is an entire $U(n)$ freedom that can be made use of and exploited when devising variational principles. In fact, a manifold structure emerges that originates from the tensor network and mode transformation degrees of freedom. Only the joint optimization fully exploits the potential of matrix-product state approaches in the study of strongly correlated fermionic condensed-matter system. It is this serious gap in the literature that is closed in this work: We overcome the prejudice that a one-dimensional embedding necessarily has to be an embedding in real space.

Setting. The Hilbert space of interacting fermions in n modes is the fermionic Fock space \mathcal{F}_n originating from the basis constituted by all Slater determinants $\{|\alpha_1, \dots, \alpha_n\rangle\}$ with $\alpha_j \in \{0, 1\}$. We denote with c_j the fermionic annihilation operator of mode j satisfying the canonical anti-commutation relations $\{c_i, c_j\} = 0$ and $\{c_i^\dagger, c_j\} = \delta_{i,j}$, with $n_j = c_j^\dagger c_j$. MPS vectors in this system take the form

$$|\psi\rangle = \sum_{\alpha_1, \dots, \alpha_n=1}^d A_{[1]}^{\alpha_1} \dots A_{[n]}^{\alpha_n} |\alpha_1 \dots \alpha_n\rangle. \quad (1)$$

We build upon ideas of adaptive fermionic mode transformations [39–41], here brought to the level of applicability to condensed-matter lattice models in two spatial dimensions.

To be specific, and to exemplify the power of our approach, the example of the spin-less interacting fermionic (spin-less Fermi-Hubbard) model

$$H = \sum_{\langle i,j \rangle} c_i^\dagger c_j + \sum_{\langle i,j \rangle} V n_i n_j, \quad (2)$$

will be in the focus of attention, where V is the interaction strength, the hopping amplitude is set to 1 and $\langle i,j \rangle$ denotes nearest neighbours $i, j \in [n]$ on a 2d cubic $N \times N$ lattice with $n = N^2$. In addition, periodic boundary condition will be imposed along both spatial dimensions, which has been considered as a major bottleneck for MPS-based approaches. This example will show-cast that state-of-the-art energies can be reached. Having said that, in the mindset of this work would be any translationally invariant Hamiltonian of the form

$$H = \sum_{i,j=1}^n t_{i,j} c_i^\dagger c_j + \sum_{i,j,k,l=1}^n v_{i,j,k,l} c_i^\dagger c_j^\dagger c_l c_k, \quad (3)$$

including local spin degrees of freedom. That is to say, the Hamiltonian is treated as a long-ranged fermionic model on a one-dimensional line equipped with a given ordering.

Methods. We optimize the single particle basis in conjunction with the MPS tensors withing multiple successive mode transformation iterations. In our implementation, a single mode transformation iteration consists of a full forward and backward DMRG sweep without basis rotations using the dynamically extended active space (DEAS) procedure [4, 33], which is followed by some number of additional sweeps with local mode transformations that adapt the single particle basis (compare Refs. [39, 40]) that also rotate the couplings in the Hamiltonian to general couplings $t'_{i,j}$ and $v'_{i,j,k,l}$. At the end of the last sweep, for the symmetric super-block configuration, we have calculated the site entropies s_i , the two-site mutual information, $I_{i,j} = s_i + s_j - s_{i,j}$, the one-particle reduced density matrix, $\rho^{(1)}$, and the occupation number distribution $\langle n_i \rangle$ with $i \in \{1, \dots, n\}$. Here $s_A = -\text{Tr}(\rho_A \ln \rho_A)$ for $A \subset [n]$ is the von-Neumann entropy of the reduced state obtained from a partial trace of the full quantum state. The eigenvalues of $\rho_{i,j}^{(1)} = \langle c_i^\dagger c_j \rangle$ define the natural occupation (NO) numbers, λ_i , and its eigenvectors the NO-basis. Based on $I_{i,j}$ we have calculated an optimized ordering using the Fiedler-vector approach [42], from $\{s_i\}$ a new complete active space vector for the DEAS procedure [33] and from $\langle n_i \rangle$ a new Hartree-Fock configuration. These together with the final rotated interaction matrices are all used as inputs for the subsequent mode transformation iteration.

The basis optimization is carried out with fixed low bond dimension $D_{\text{opt}} \simeq 64$ and 256 or with a systematic increase of D_{opt} as will be discussed below. After convergence is reached large scale DMRG calculations are performed with increasing bond dimension or using the *dynamic block state selection (DBSS)* approach with fixed truncation error threshold [43, 44]. We denote these data as (D_{opt}, D) or $(D_{\text{opt}}, \varepsilon_{\text{tr}})$, respectively. In addition, a given quantity obtained from a calculation in the optimized basis will be indicated with a tilde.

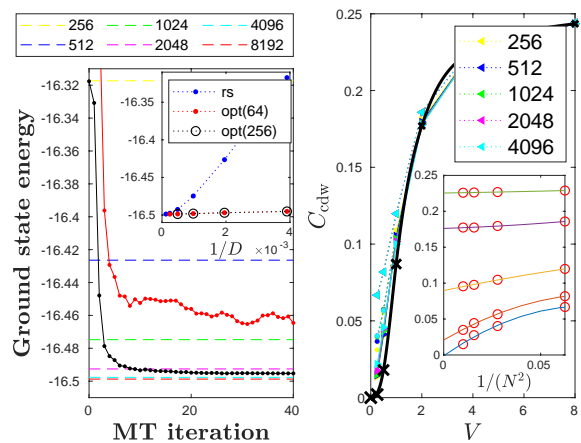


FIG. 1. (Left panel) convergence of the ground state energy for the half-filled 6×6 spin-less fermion model for $V = 1$ as a function of mode transformation iterations for fixed bond dimension of $D_{\text{opt}} = 64$ and 256 is shown by red and black curves, respectively. In the inset, the scaling of the ground state energy with inverse bond dimension obtained in the real space basis and in the optimized basis for $D_{\text{opt}} = 64$ and 256 are shown, respectively. (Right panel) Charge density wave order parameter for the $N \times N$ half-filled spin-less fermion model as a function of V for various values of D obtained in the real space basis. Black crosses indicate extrapolated data to the $N \rightarrow \infty$ limit obtained in the optimized basis and using finite size scaling data shown for various interaction strengths in the inset (curves correspond from bottom to top to $V = 0.25, 0.5, 1, 2, 4$, and 8). The solid black line is a spline fit to the extrapolated data. The error in the extrapolated data is indicated by the symbol sizes.

Numerical results. Our systematic error and convergence analysis will be given for the 6×6 two dimensional lattice, since highly accurate reference data with the real space basis can also be generated. For larger system sizes, namely for 8×8 and 10×10 , only final results will be discussed (further numerical data and figures are presented in the supplements).

In the left panel of Fig. 1, we show the ground state energy $\tilde{E}(D_{\text{opt}})$ for $V = 1$ as a function of mode transformation iterations using fixed bond dimensions $D_{\text{opt}} = 64$ and 256. Reference energies $E(D)$ obtained in the real space basis are indicated with dashed lines for various bond dimensions up to $D = 8192$. It obvious indeed that exploiting mode transformations, $\tilde{E}(64)$ gets significantly below $E(512)$ even after the fourth iteration step and $\tilde{E}(256)$ is below $E(2048)$. For further numerical results emphasizing how faithfully information beyond the ground state energy can be reproduced and predicted in the optimized basis, we refer to Fig. 3 in the supplements. In the inset of the left panel of Fig. 1, we depict the ground state energy as an inverse of the bond dimension for the real space basis and for the optimized basis with $D_{\text{opt}} = 64$ and 256. In the latter case, $\tilde{E}(D_{\text{opt}}, D)$ lie on the top of each other, indicating that the optimal basis has been found with $D_{\text{opt}} = 64$ already (red dots in black circles).

For larger system sizes, the improvements are even more remarkable as is shown in Fig. 4 in the supplements for the

8×8 lattice for different values of D_{opt} and for $V = 1$ and 8. Here, $\tilde{E}(256)$ is already lower than $E(8192)$. In addition, reliable extrapolation with $1/D$ to the $D \rightarrow \infty$ truncation free limit would require even significantly larger bond dimensions for the real space basis. In contrast to this, in case of the optimized basis, this is no longer an issue since $\tilde{E}(256, D)$ is basically a flat curve. Our very accurate results have been obtained for a torus geometry. This reduces finite size effects significantly and much smaller systems sizes could lead to a reliable extrapolation to the thermodynamic limit (see Tab. I).

The remarkable superiority of the optimized basis over the real space basis is due to the dramatic reduction of the entanglement. As an indication of this, we depict the block entropy $s[l]$, $l \in \{1, \dots, n\}$ in the left panel of Fig. 2 for various selected mode transformation iterations. Here, the maximum of $s[l]$ reduced by a full order of magnitude, as can be seen by comparing the blue (real space basis) and the black (optimized basis) curves. In addition, artifacts of the snake-like mapping of the two-dimensional lattice in real space into the one-dimensional MPS topology apparent in the blue curve are completely diminished by the basis optimization resulting in a smooth and highly symmetric profile (additional data is available in the supplements in Fig. 5). The iterative error norm of the block entropy measured between two subsequent mode transformation iterations, $\|s_{[l]}^{k+1} - s_{[l]}^k\|$ converges to 10^{-5} - 10^{-4} which can also be used as a criterion when to terminate the basis optimization. For larger V values, the reduction is even more pronounced, leading to a state that is close to a Slater determinant. In the right panel, the maximum of $s[l]$ for $l \in \{1, \dots, n\}$ – which typically appears near the center of the chain – is laid out for various D values for the real space basis and for the optimized one. While a strong D dependence for $V \leq 2$ is clearly visible in the real space basis, the curves basically fall on top of each other for the optimized basis. The small peak for $0 \leq V \leq 2$ signals the residual entanglement that cannot be removed by basis optimization which also controls the required bond dimension and thus the computational complexity. As a benchmark we have performed DMRG calculations using the DBSS approach with minimum bond dimension $D_{\text{min}} = 1024$ and a truncation error threshold $\varepsilon_{\text{tr}} = 10^{-7}$. An agreement up to four digits has been obtained compared to the real space energy reference data calculated with $D = 8192$, but we have gained a speedup by a full order of magnitude.

Through the course of basis optimization, the residual quantum correlations that have to be captured by the tensor network ansatz are significantly reduced. As a further proxy for this behaviour, one may investigate the sum of the single mode von-Neumann entropies $I_{\text{tot}} = \sum_i s_i$ that is reduced drastically, while pair-wise correlations reflected by $I_{i,j}$ get very much localized (for additional numerical data see Fig. 7). In addition, the investigation of the one-particle reduced density matrix shows that the optimized basis converges to the natural orbital basis as λ_i and $\langle n_i \rangle$ tend to lie on the top of each other (Fig. 7). Therefore, here the final basis is the nat-

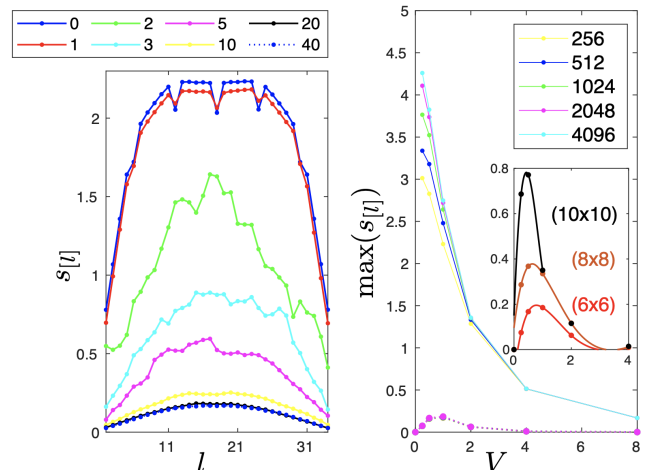


FIG. 2. (Left panel) block entropy for the 6×6 half-filled spin-less fermion model for $V = 1$ for some selected mode transformation iterations with $D_{\text{opt}} = 256$, i.e., for the 0th, 1th, 2nd, 3rd, 5th, 10th, 20th, 40th iterations. (Right panel) maximum of the block entropy as a function of V for various D values and for the real space basis (solid lines) and for the optimized basis (dashed lines). In the inset, this is shown for various systems sizes obtained with the optimized basis and DMRG with $D_{\text{min}} = 1024$ and $\varepsilon_{\text{tr}} = 10^{-6}$. Here a spline is fitted as guide for the eye through the data points.

ural orbital basis, but the underlying basis has been systematically rotated by each mode transformation iterations. Therefore, as an alternative approach, we have also tested rotations based on the natural orbitals at the end of each mode transformation iteration, but encountered a very unstable performance in agreement with earlier attempts [45] (see Fig. 6).

Phase diagram. The power of our approach allows us to attack the physical properties such as the phase diagram of the system as well. In the limit of strong interactions, the model maps onto the anti-ferromagnetic Ising model in two dimensions and a *charge density wave (CDW)* phase develops. Since the hopping is restricted to nearest neighbours only, the Fermi surface takes the form of a square and perfect nesting together with Van Hove singularities providing strong arguments for an Ising transition into the CDW-ordered phase at $V_c = 0$ [46, 47]. Furthermore, investigations within the Hartree-Fock approximation lead to an exponentially small order parameter in the weak coupling limit and the $1/d$ corrections starting from the $d = \infty$ limit, where Hartree-Fock theory becomes exact, provides only very small quantitative corrections in $d = 3$ and even in $d = 2$ [48]. For $d = 2$ this indicates a transition at $V_c = 0$ and that the charge density wave order parameter is an exponential function of V in the weak coupling limit. Note, however, that these simple arguments can break down as in the case of spin-less fermions in one spatial dimension, $d = 1$, where the model reduces to the integrable Heisenberg model and has a transition at finite V_c [48]. Ref. [49] has shown that there is a direct transition between the homogeneous and the CDW phases governed by phase separation, and a finite $V_c \simeq 0.5$ is suggested based

on their obtained phase diagram. Their underlying arguments, however, have been derived for finite doping, thus an exponentially closing phase boundary between the CDW and phase separated phases together with $V_c = 0$ cannot be ruled out.

In order to investigate the transition we first analyze the block entropy profiles for larger system sizes using the optimized basis and find that the peak for $V \leq 1$ remains and its height increases with system size as is shown in the inset of Fig. 2. The center of the peak extracted from the spline fits ($V = 0.78, 0.65, 0.43$ for $N = 6, 8, 10$) tends to shift to $V = 0$ with $1/N^2$ while a finite value could have signaled a quantum phase transition [50] at finite V_c . We also compute the CDW order parameter [51] as expectation value of $C_{\text{cdw}} = (1/N^4) \sum_{i,j} \eta_{i,j} (n_i - 1/2)(n_j - 1/2)$ directly, where $n_i = c_i^\dagger c_i$ in the real space basis and $\eta_{i,j}$ is a phase matrix with elements ± 1 in a checker-board arrangement on the 2d-lattice. The real-space simulations show that for large values of V , $\langle C_{\text{cdw}} \rangle$ takes a finite value while for $V = 0$ it has to vanish as can be seen in the right panel of Fig. 1. The apparent finite size and D dependencies do not allow us to conclusively decide upon the behaviour of $\langle C_{\text{cdw}} \rangle$ for $V \leq 1$. Alternatively, the density-density correlation function can also be taken from the elements of the one- and two-particle reduced density matrices. The latter one has entries $\rho_{i,j,k,l}^{(2)} = \langle c_i^\dagger c_j^\dagger c_k c_l \rangle$ which can also be calculated efficiently by the DMRG method [52]. Measuring these in the optimized basis and back-rotating to the real space basis, we found an agreement up to four digits between $\langle \tilde{C}_{\text{cdw}} \rangle$ and the real space reference for $N = 4$ and 6. For $N = 8$ and $V \leq 1$ the two data sets, however, began to deviate and $\langle \tilde{C}_{\text{cdw}} \rangle$ possesses a much weaker D dependence. Finite size scaling of the large scale DMRG data obtained with $M_{\text{min}} = 1024$ and $\varepsilon_{\text{tr}} = 10^{-6}$ is shown in the inset of Fig. 1 right panel for various V values. For large V the curves scale to finite values in the thermodynamic limit, while for $V \leq 1$ they show a slight downward curvature. For $V = 0.25$ the extrapolated value of C_{cdw} of the order of 10^{-3} which might either be considered as being zero. Alternatively, after a rough extrapolation with $1/N$ and a spline fit on the extrapolated data (black crosses in the figure) an exponential opening of $\langle \tilde{C}_{\text{cdw}} \rangle$ at $V_c = 0$ can also be obtained. This functional form agrees to the one reported in Ref. [48] after some re-scaling and it is shown by a black curve in the right panel of Fig. 1. Our approach hence pushes forward the capacity of the MPS based approaches to capture two dimensional strongly correlated systems significantly. Our results are in close agreement with analytic expectations (while some details remain open).

Conclusion. In this work, we have demonstrated that MPS approaches, extending known DMRG methods, are surprisingly powerful for the simulation of two-dimensional quantum many body systems even imposing periodic boundary condition along both spatial dimensions. This is possible if only the key insight is acknowledged that one is not forced to do a local basis representation. Algorithmically, this is achieved by adaptively finding the optimal basis via fermionic mode transformation, optimizing over a larger manifold than

that of MPS, which leads to a dramatic reduction of the correlations and entanglement in the system. A strongly interacting model in the real space basis thus can be converted to a weakly correlated problem in the optimized basis. Due to the torus geometry, finite size dependence is significantly reduced and intermediate system sizes make it possible to carry out more reliably extrapolations to the thermodynamic limit. In fact, for the two-dimensional translationally invariant spinless fermion model, our results strongly suggest the presence of a quantum phase transition at $V_c \simeq 0$, but the very small values of the charge density order parameter obtained numerically in the weak coupling limit leaves an uncertainty in our conclusion. The inclusion of a hopping between next nearest neighbours, however, would distort the square Fermi-surface and perfect nesting over an extended region of the momentum space will be destroyed. This is expected to have a major effect, and divergencies in the susceptibilities might be removed and a finite V_c is even more likely. This behaviour also shares features with the phase diagram of spin-less fermions on the honeycomb lattice [53]. Then, physical properties of the transformed basis are of key importance. In general, the ground state energy cannot be written as a sum of energies of quasi-particle states except for special cases. The $V = 0$ and large V limits belong to the latter case (the ground state is a product state), but the residual block entropy for $0 < V \leq 2$ reflects the general scenario. Excitation energies, however, can be expressed through quasi-particle excitations (as forthcoming work will explore).

Our basis optimization is very robust, it can be carried out with low bond dimension, and calculations using the optimized basis can easily lead to an order of magnitude speedup in computational time. In addition, our method is stable for weakly and strongly interacting systems, in general, while standard approaches, like basis transformation based on natural orbitals, that have been attempted earlier have major limitations and drawbacks. Remarkably, the optimized basis for the spin-full Hubbard model does not resemble the characteristics of natural orbitals which reflects the existence of much stronger residual correlations in the system (as forthcoming work will explore). Conceptually most importantly, our work overcomes the deep misconception that lower-dimensional embeddings necessarily have to capture some kind of locality. Once this prejudice is overcome, acknowledging that fermionic mode transformations are not restricted to one-dimensional embeddings, mode reductions can be brought to a new level. Due to the polynomial scaling of the non-local DMRG [54] effort as $O(D^3 n^3) + O(D^2 n^4)$, a reduction of D by one or two orders of magnitude will render DMRG competitive for simulating higher dimensional and complex problems as well. Our approach has the potential to become a standard protocol for tensor network methods.

Acknowledgements. J. E. has been supported by the Templeton Foundation, the ERC (TAQ), the DFG (EI 519/15-1, EI519/14-1, CRC 183 Project B01), and the European Union's Horizon 2020 research and innovation program under Grant Agreement No. 817482 (PASQuanS). Ö. L. has been sup-

ported by the Hungarian National Research, Development and Innovation Office (NKFIH) through Grant No. K120569, by the Hungarian Quantum Technology National Excellence Program (Project No. 2017-1.2.1-NKP-2017-00001). Ö. L. also acknowledges financial support from the Alexander von Humboldt foundation and useful discussions with Jenő Sólyom, Karlo Penc, and Florian Gebhard. L. V. has been supported by the Czech Science Foundation through Grant No. 18-18940Y.

-
- [1] R. Orus, *Ann. Phys.* **349**, 117 (2014).
 [2] F. Verstraete, J. I. Cirac, and V. Murg, *Adv. Phys.* **57**, 143 (2008).
 [3] J. Eisert, *Mod. Sim.* **3**, 520 (2013).
 [4] S. Szalay, M. Pfeiffer, V. Murg, G. Barcza, F. Verstraete, R. Schneider, and Ö. Legeza, *Int. J. Quant. Chem.* **115**, 1342 (2015).
 [5] J. Eisert, M. Cramer, and M. B. Plenio, *Rev. Mod. Phys.* **82**, 277 (2010).
 [6] S. R. White, *Phys. Rev. Lett.* **69**, 2863 (1992).
 [7] S. R. White and R. M. Noack, *Phys. Rev. Lett.* **68**, 3487 (1992).
 [8] U. Schollwöck, *Ann. Phys.* **326**, 96 (2011).
 [9] M. Fannes, B. Nachtergaele, and R. F. Werner, *Commun. Math. Phys.* **144**, 443 (1992).
 [10] D. Perez-Garcia, F. Verstraete, M. M. Wolf, and J. I. Cirac, *Quantum Info. Comput.* **7**, 401 (2007).
 [11] S. Rommer and S. Östlund, *Phys. Rev. B* **55**, 2164 (1997).
 [12] M. B. Hastings, *J. Stat. Mech.* **2007**, P08024 (2007).
 [13] I. Arad, A. Kitaev, Z. Landau, and U. Vazirani, arxiv:1301.1162.
 [14] N. Schuch, M. M. Wolf, F. Verstraete, and J. I. Cirac, *Phys. Rev. Lett.* **100**, 030504 (2008).
 [15] U. Schollwöck, *Rev. Mod. Phys.* **77**, 259 (2005).
 [16] T. Nishino, “Unofficial DMRG, MPS, TPS, and MERA home page,” [Http://quattro.phys.sci.kobe-u.ac.jp/dmrg/condmat.html](http://quattro.phys.sci.kobe-u.ac.jp/dmrg/condmat.html).
 [17] G. Vidal, *Phys. Rev. Lett.* **91**, 147902 (2003).
 [18] A. J. Daley, C. Kollath, U. Schollwöck, and G. Vidal, *J. Stat. Mech.* **2004**, P04005 (2004).
 [19] J. Haegeman, C. Lubich, I. Oseledets, B. Vandereycken, and F. Verstraete, *Phys. Rev. B* **94**, 165116 (2016).
 [20] F. Verstraete, J. J. Garcia-Ripoll, and J. I. Cirac, *Phys. Rev. Lett.* **93**, 207204 (2004).
 [21] A. H. Werner, D. Jaschke, P. Silvi, M. Kliesch, T. Calarco, J. Eisert, and S. Montangero, *Phys. Rev. Lett.* **116**, 237201 (2016).
 [22] V. Khemani, F. Pollmann, and S. L. Sondhi, *Phys. Rev. Lett.* **116**, 247204 (2016).
 [23] F. Verstraete and J. I. Cirac, cond-mat:0407066.
 [24] T. Barthel, C. Pineda, and J. Eisert, *Phys. Rev. A* **80**, 042333 (2009).
 [25] C. V. Kraus, N. Schuch, F. Verstraete, and J. I. Cirac, *Phys. Rev. A* **81**, 052338 (2010).
 [26] I. Pižorn and F. Verstraete, *Phys. Rev. B* **81**, 245110 (2010).
 [27] P. Corboz, *Phys. Rev. B* **93**, 045116 (2016).
 [28] S. Yan, D. A. Huse, and S. R. White, *Science* **332**, 1173 (2011).
 [29] S. Depenbrock, I. P. McCulloch, and U. Schollwöck, *Phys. Rev. Lett.* **109**, 067201 (2012).
 [30] E. M. Stoudenmire and S. R. White, *An. Rev. Cond. Mat. Phys.* **3**, 111 (2012).
 [31] T. Xiang, *Phys. Rev. B* **53**, R10445 (1996).
 [32] S. Nishimoto, E. Jeckelmann, F. Gebhard, and R. M. Noack, *Phys. Rev. B* **65**, 165114 (2012).
 [33] Ö. Legeza and J. Sólyom, *Phys. Rev. B* **68**, 195116 (2003).
 [34] Ö. Legeza, F. Gebhard, and J. Rissler, *Phys. Rev. B* **74**, 195112 (2006).
 [35] V. Murg, F. Verstraete, Ö. Legeza, and R. M. Noack, *Phys. Rev. B* **82**, 205105 (2010).
 [36] G. Ehlers, J. Sólyom, Ö. Legeza, and R. M. Noack, *Phys. Rev. B* **92**, 235116 (2015).
 [37] J. Motruk, P. M. Zaletel, S. K. R. Mong, and F. Pollmann, *Phys. Rev. B* **93**, 155139 (2016).
 [38] G. Ehlers, S. R. White, and R. M. Noack, *Phys. Rev. B* **95**, 125125 (2017).
 [39] C. Krumnow, L. Veis, Ö. Legeza, and J. Eisert, *Phys. Rev. Lett.* **117**, 210402 (2016).
 [40] C. Krumnow, *Detecting and understanding efficient structures in finite fermionic systems*, Ph.D. thesis, Freie Universität Berlin (2018).
 [41] C. Krumnow, J. Eisert, and Ö. Legeza, arXiv:1904.11999 (2019).
 [42] G. Barcza, Ö. Legeza, K. H. Marti, and M. Reiher, *Phys. Rev. A* **83**, 012508 (2011).
 [43] Ö. Legeza, J. Röder, and B. A. Hess, *Phys. Rev. B* **67**, 125114 (2003).
 [44] Ö. Legeza and J. Sólyom, *Phys. Rev. B* **70**, 205118 (2004).
 [45] J. Rissler, R. M. Noack, and S. R. White, *Chem. Phys.* **323**, 519 (2006).
 [46] J. Sólyom, *Fundamentals of the Physics of Solids, Vol. 3, Normal, Broken-Symmetry, and Correlated Systems* (Springer, 2011).
 [47] W. Metzner, M. Salmhofer, C. Honerkamp, V. Meden, and K. Schönhammer, *Rev. Mod. Phys.* **84**, 299 (2012).
 [48] E. Halvorsen, G. S. Uhrig, and G. Czycholl, *Z. Phys. B* **94**, 291 (1994).
 [49] G. S. Uhrig and R. Vlaming, *Phys. Rev. Lett.* **71**, 271 (1993).
 [50] Ö. Legeza and J. Sólyom, *Phys. Rev. Lett.* **96**, 116401 (2006).
 [51] L. Wang, P. Corboz, and M. Troyer, *New J. Phys.* **16**, 103008 (2014).
 [52] D. Zgid and M. Nooijen, *J. Chem. Phys.* **128**, 144115 (2008).
 [53] S. Capponi, *J. Phys.: Condens. Matter* **29**, 043002 (2017).
 [54] S. R. White and R. L. Martin, *J. Chem. Phys.* **110**, 4127 (1999).

Supplemental material: Additional data for larger systems

In this section, we present additional numerical data together with further scaling properties obtained for larger system sizes.

Error analysis of the one particle reduced density matrix

In order to investigate how faithfully information beyond the ground state energy can be reproduced and predicted in the optimized basis, we depict in Fig. 1 the operator norm of the difference of the one particle reduced density matrix $\widetilde{\rho}^{(1)}(D_{\text{opt}})$ over the mode transformation iterations and the

real space reference data $\rho^{(1)}(8192)$. Using the optimized basis, we also show the result for $\widetilde{\rho}^{(1)}(D_{\text{opt}}, D)$ with increasing bond dimension D , using different symbols. These latter data sets are basically the same for $D_{\text{opt}} = 64$ and 256, thus the optimal basis has already been obtained with the lower D_{opt} value (see Fig. 3). The error norms obtained with the real space basis are again much larger as indicated by the dashed lines. It is worth to remark that the error norm is less meaningful for very large bond dimensions since $\widetilde{E}(256, 4096)$ is below $E(8192)$ rendering $\widetilde{\rho}^{(1)}(256, 4096)$ potentially more accurate than $\rho^{(1)}(8192)$.

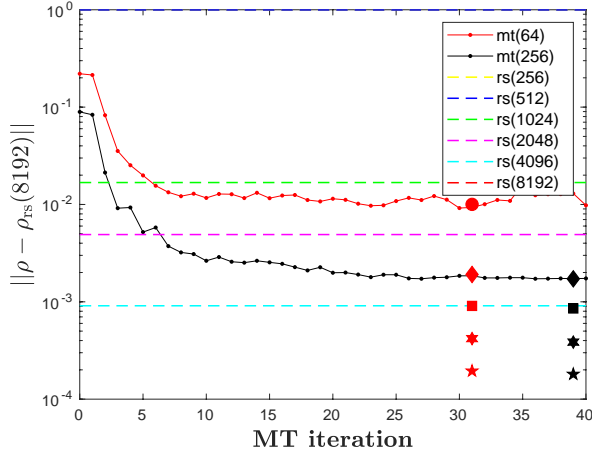


FIG. 3. Error norm of the one-particle reduced density matrix with respect to the reference obtained with the real space basis with $D = 8192$. Red and black symbols show result for $D = 64, 256, 512, 1024, 2048$ but using the optimized basis for $D_{\text{opt}} = 64$ and 256, respectively. For both quantities reference data obtained with the real space basis for various D values up to 8192 are shown with dashed lines and labeled as $\text{rs}(D)$.

Further numerical results for the ground state energy of the half-filled $N \times N$ spin-less fermion model

In Fig. 4, we present further numerical results for the ground state energy of the half-filled 8×8 spin-less fermion model, and obtained bond energies are summarized up to lattice sizes 10×10 in Tab. I.

	0.25	0.5	1	2	4	8
4×4	-0.6636	-0.5845	-0.4518	-0.2878	-0.1591	-0.0823
6×6	-0.6847	-0.5992	-0.4583	-0.2911	-0.1601	-0.0825
8×8	-0.6947	-0.6059	-0.4604	-0.2912	-0.1601	-0.0825
10×10	-0.6983	-0.6080	-0.4605	-0.2912	-0.1601	-0.0825

TABLE I. Convergence of the bond energy, E/N^2 , with system size for various V values. DMRG results were obtained using the optimized basis and the DBSS procedure with $M_{\text{min}} = 1024$, and $\epsilon_{\text{tr}} = 10^{-6}$.

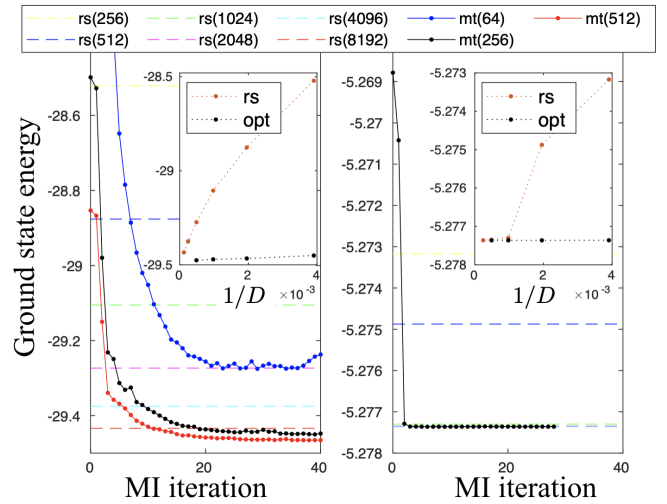


FIG. 4. Convergence of the ground state energy for the half-filled 8×8 spin-less fermion model as a function of mode transformation iterations for fixed bond dimension of $D_{\text{opt}} = 64, 256$ and 512 is shown by blue, red and black curves, respectively for $V = 1$ (left panel) and for $V = 8$ (right panel). Reference data obtained in the real space basis for D up to 8192 are shown with dashed lines. In the inset, the scaling of $E(D)$ and $\widetilde{E}(256, D)$ with the inverse bond dimension is shown.

Further numerical results for the ground state block entropy profiles of the half-filled 8×8 spin-less fermion model

In Fig. 5, we show further numerical results on the optimized block entropy profiles using different optimization parameter sets.

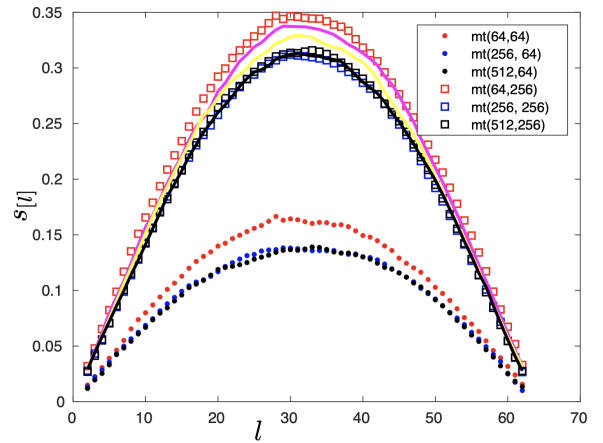


FIG. 5. (Left panel) The block entropy $s_{[l]}(D_{\text{opt}}, D)$ for the half-filled 8×8 spin-less fermion model for $V = 1$ for various $\{D_{\text{opt}}, D\}$ sets. Solid lines correspond to mode transformation iterations using $D_{\text{opt}} = 256$, but starting from a basis already optimized with $D_{\text{opt}} = 64$. The finally optimized profile lie on top of the the profile optimized with $D_{\text{opt}} = 256$, starting from the real space basis. Therefore, in practice, the basis can be optimized by systematically increasing D_{opt} until the entropy profile fully converges.

Mode transformation analysis using rotations based on natural orbitals for the half-filled 8×8 spin-less fermion model

Since the final basis is the natural orbital basis (see Fig. 6), one might think that a natural step is to aim at identifying a globally optimal single particle basis could be more directly based on natural orbitals, i.e., by instead of using the local updates to the single particle basis one could rotate to the natural orbitals at the end of each mode transformation iteration. Such an approach has already been tested for quantum chemical applications [45], but a very unstable performance has been reported. In fact, we have also found that in the small- V limit such an approach works acceptably, but for larger V values it breaks down (see Fig. 6). The reason is that for small V the optimal orbitals are Hartree-Fock like orbitals, while for large V values localized orbitals seem to be more optimal. Our novel method based on fermionic mode transformation is, however, stable for all V values. Importantly, it can also be used in general for interacting quantum many body systems.

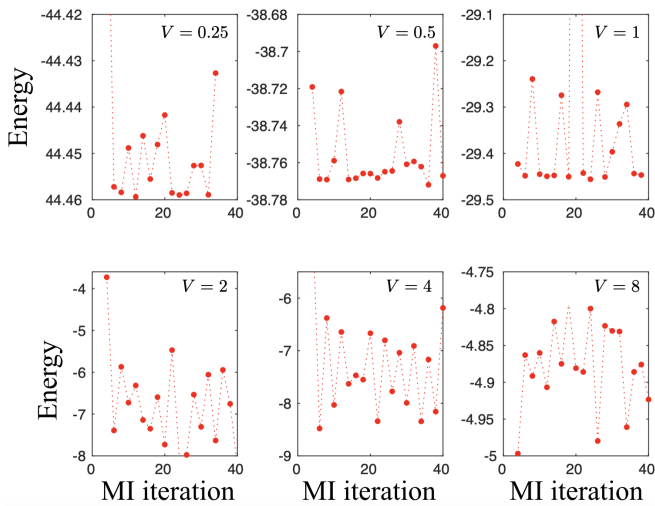


FIG. 6. Convergence of the ground state energy for the half-filled 8×8 spin-less fermion model as a function of mode transformation iterations with fixed bond dimension of $D_{\text{opt}} = 256$ for various V values if we rotate to the natural orbitals after the 7th sweep of each iteration instead of using the local updates and perform another 7 sweeps to obtain a converged ground state in the current rotated basis in order to determine the optimal ordering for the next iteration. Therefore, each iteration based on natural orbitals corresponds to every second iteration based on fermionic mode transformation.

Monitoring various entropic quantities through the course of mode transformations

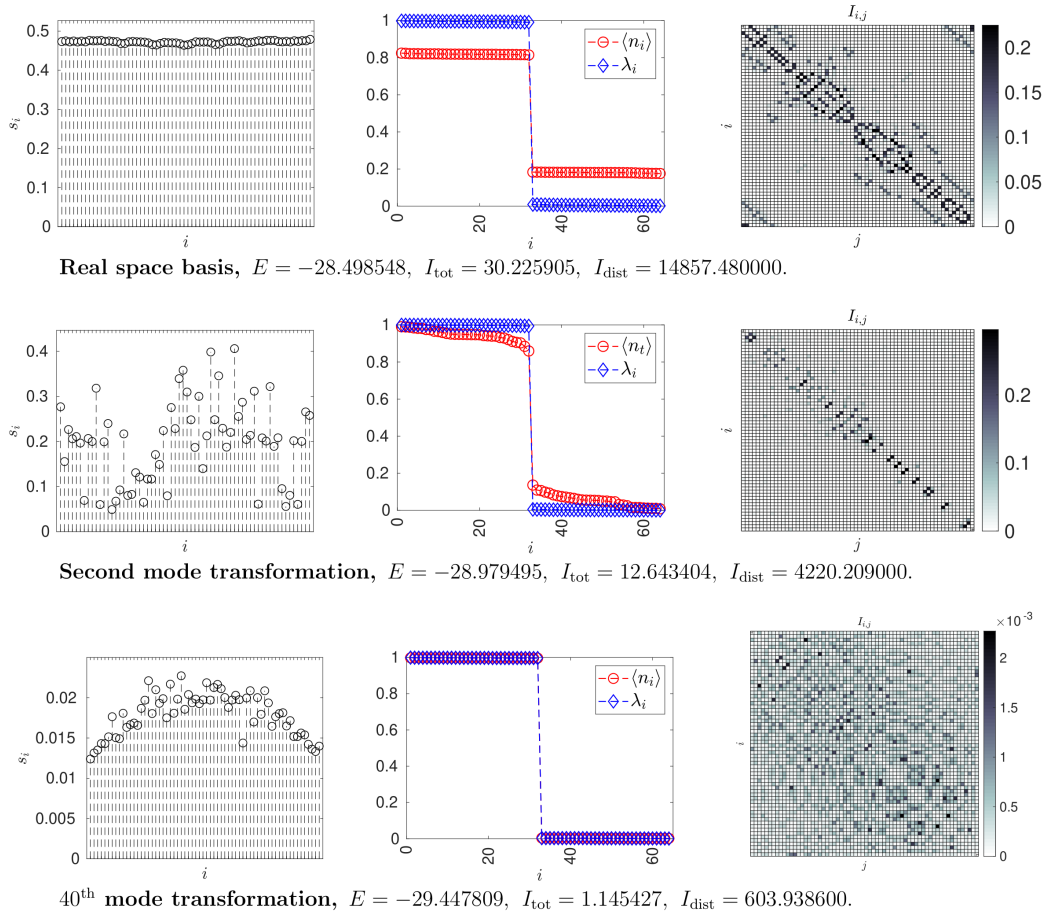


FIG. 7. Site entropy profile s_i , sorted values of the natural orbital occupation numbers, λ_i , occupation number, $\langle n_i \rangle$ and mutual information, $I_{i,j}$ for the real space basis (first row), and for the 2nd and 40th mode transformation iterations for the half-filled 8×8 spin-less fermion model for $V = 1$ and $D_{\text{opt}} = 256$. The ground state energy, the sum of the site entropy I_{tot} , and the entanglement distance $I_{\text{dist}} = \sum_{i,j} I_{i,j} |i-j|^2$, are printed below the corresponding panels.